The Journal of Chemical Physics

RESEARCH ARTICLE | NOVEMBER 15 2022

# Thermodiffusion of polymer solutions and colloidal dispersions in mixed solvents

D. Sommermann; M. Schraml; W. Köhler



*J. Chem. Phys.* 157, 194903 (2022)
https://doi.org/10.1063/5.0128626

The Journal of Chemical Physics ARTICLE scitation.org/journal/jcp

# Thermodiffusion of polymer solutions and colloidal dispersions in mixed solvents

Cite as: J. Chem. Phys. 157, 194903 (2022); doi: 10.1063/5.0128626
Submitted: 29 September 2022 • Accepted: 26 October 2022 •
Published Online: 15 November 2022



D. Sommermann, M. Schraml, and W. Köhler[a)]

## AFFILIATIONS

Physikalisches Institut, Universität Bayreuth, D-95440 Bayreuth, Germany

[a)]Author to whom correspondence should be addressed: werner.koehler@uni-bayreuth.de

## ABSTRACT

Two-color optical measurements of thermodiffusion in ternary mixtures frequently suffer from ill-conditioned contrast factor matrices, whose inversion leads to very large experimental errors. In this contribution, we show how the error amplification can be avoided in situations where *a priori* knowledge about the directions of the eigenvectors of the diffusion matrix is available. We present optical beam deflection experiments on solutions of the polymer polystyrene of $M_w$ = 4880 g/mol in a mixed solvent of toluene and cyclohexane. In this system, the two diffusion eigenvalues differ by almost one order of magnitude. The large eigenvalue can be attributed to the interdiffusion of the two solvents and the small one to the polymer diffusion relative to the mixed solvent. The pre-selection of the eigenvectors renders the method stable against fluctuations of the experimental parameters. Both the diffusion and the Soret coefficients attributed to the two modes agree very well with the respective values of corresponding binary mixtures.





## I. INTRODUCTION

Most measurements of thermodiffusion and Soret coefficients are nowadays performed by optical detection of refractive index changes.[1,2] In the case of binary mixtures in the dense liquid state with large Lewis numbers,[3] the transient signals that follow a temperature perturbation contain two contributions that are well separated on the time axis and can be attributed to the fast thermal and the slow solutal part. Already for ternaries, let alone higher multicomponent mixtures, the complexity grows tremendously. The number of independent solutal transport coefficients increases from one diffusion and one thermodiffusion coefficient to four independent diffusion and two thermodiffusion coefficients. The dynamics of the solutal signal becomes bimodal with the two time constants determined by the eigenvalues of the 2 × 2-diffusion matrix. While these two eigenvalues can be obtained from a single transient signal, the eigenvectors of the diffusion matrix are not known. The disentanglement of the concentrations requires the measurement with a second wavelength and the inversion of the so-called contrast factor matrix.[4–8] The latter is frequently ill-conditioned,[5,8,9] which can lead to a huge error-amplification after the transformation from the refractive index to the concentration space. In unfavorable situations, even very precise optical measurements yield only crude estimates of Soret and thermodiffusion coefficients.[9,10]

There is no easy solution for the inversion problem in the general case although concepts such as the Soret vectors[11] can be very helpful. In this contribution, we will, however, show that reasonable *a priori* assumptions can change the situation completely for certain systems. We will discuss the case of strongly asymmetric ternary systems of, e.g., a large polymer or colloid dispersed in a mixed solvent of small molecules. The two diffusion eigenvalues in such systems are frequently well separated, and the fast mode and the slow mode are typically attributed to the diffusion of the solvent and the polymer, respectively.[12,13]

Despite these reasonable assumptions, the whole problem has never fully been worked out. Here, we will treat this special case using the established theory for ternary mixtures. We will show that the identification of these two modes fixes the eigenvectors of the diffusion matrix and, hence, the diagonalizing transformation of the coupled diffusion equations for the two concentration variables. The knowledge of this transformation eliminates the need for the inversion of the contrast factor matrix. It solves the problem of the high condition number and reduces the transformation to the concentration space from a two-dimensional to a one-dimensional

problem. Besides the Soret coefficients for all three components as derived from the asymptotic steady state, we will also analyze the two solutal modes independently and compare their transport properties with the ones of the corresponding binaries. We will discuss experiments performed by optical beam deflection (OBD), but the arguments equally well hold for other optical techniques, e.g., thermal diffusion forced Rayleigh scattering (TDFRS)[14,15] or optical digital interferometry (ODI).[16]

We present experiments for an asymmetric ternary model system, namely, a polymer (polystyrene, PS) in mixtures of the two solvents toluene (Tol) and cyclohexane (cHex). The polymer represents a large entity that is dispersed at a relatively low concentration in a binary solvent composed of small molecules.

## II. THEORY

### A. Diffusion eigenvectors

Thermodiffusion in ternary mixtures is described by two coupled diffusion equations for the two independent concentrations (mass fractions) $c_1$ and $c_2$ as follows:[4,17]

$$\frac{\partial \underline{c}}{\partial t} = \underline{\underline{\mathbf{D}}}(\nabla^2 \underline{c}) + \underline{D'_T}\nabla^2 T. \tag{1}$$

An underline represents a vector in the 2d-concentration space, such as the concentrations $\underline{c} = (c_1, c_2)^{\mathrm{T}}$ or the thermodiffusion coefficients $\underline{D'_T} = (D'_{T,1}, D'_{T,2})^{\mathrm{T}}$. The diffusion matrix $\underline{\underline{\mathbf{D}}}$ with entries $D_{ij}$ $(i,j = 1,2)$ has the two eigenvalues $\hat{D}_1$ and $\hat{D}_2$. The concentrations are decoupled by a transformation $\underline{C} = \underline{\underline{\mathbf{V}}}^{-1}\underline{c}$ with the eigenvector matrix $\underline{\underline{\mathbf{V}}}$ of the diffusion matrix. The latter is diagonalized by $\underline{\underline{\hat{\mathbf{D}}}} = \underline{\underline{\mathbf{V}}}^{-1}\underline{\underline{\mathbf{D}}}\,\underline{\underline{\mathbf{V}}}$.

As described in the introduction, the eigenvalues of $\underline{\underline{\mathbf{D}}}$ are directly determined from a bimodal fit of the solutal optical signal recorded with a single laser wavelength. The two eigenvectors, however, are not easily obtainable even in two-color experiments, which, in principle, should contain sufficient information. In the following, we will use *a priori* assumptions for the direction of the eigenvectors that appear reasonable for the here discussed system. Of course, these assumptions need to be justified by the final result.

The ternary system under consideration shall consist of, e.g., a polymer or a colloid as component 1 dissolved in a binary mixture of small molecules as components 2 and 3. For the sake of simplicity, we will frequently call the first component just "the polymer." Our treatment is guided by the idea that the fast mode can be attributed to the interdiffusion of the two solvents at constant polymer concentration. The slow mode, on the other hand, is due to the polymer diffusing with respect to the mixed solvent, whose composition is not affected by the slower diffusing polymer. As usual, we take $c_3 = 1 - c_1 - c_2$ as the dependent and $c_1$ and $c_2$ as the independent concentrations.

Figure 1 shows the Gibbs triangle of our ternary system for three different compositions $c_3/c_2 = 4$, $c_3/c_2 = 1$, and $c_3/c_2 = 0.5$ of the binary solvent and a fixed polymer concentration of $c_1 = 0.2$. Note that we are more interested in the limit $c_1 \ll c_2 + c_3$, but here we have chosen the relatively high polymer concentration of 0.2 for the sake of clarity of the figure.

The two postulated eigenvectors of the diffusion matrix are $\underline{v}_1$ and $\underline{v}_2$. The first one corresponds to the fast interdiffusion of $c_2$

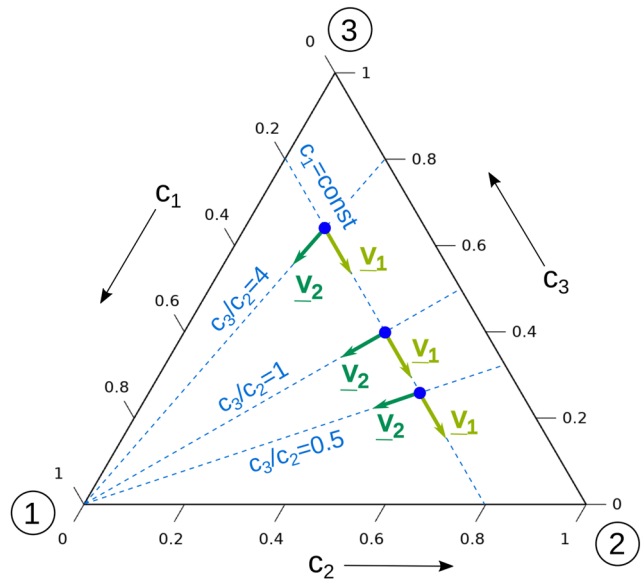


**FIG. 1.** Gibbs triangle of a ternary mixture of a polymer or colloid (1) and a binary solvent (2 and 3). $\underline{v}_1$ and $\underline{v}_2$ are the two eigenvectors of the diffusion matrix for three different compositions $r = c_3/c_2$ of the binary solvent.

and $c_3$ at constant polymer concentration $c_1$ with eigenvalue $\hat{D}_1$. The second one belongs to the eigenvalue $\hat{D}_2$ and points along the direction of the polymer diffusion with respect to the binary solvent of constant composition ratio $c_3/c_2$.

For the following discussion, it is advantageous to represent the eigenvectors in the 2d-space of the independent concentrations $c_1$ and $c_2$. This is shown in Fig. 2 for the special case $r = c_3/c_2 = 0.5$. The fast mode relates to a change in $c_2$ on expense of the dependent component $c_3$ at constant $c_1$. Hence, $\underline{v}_1$ points along the $c_2$ axis. The slow mode corresponds to a change $\delta c_1$ of the polymer concentration that is compensated by the combined concentration change in the two solvents, hence $\delta c_1 = -\delta c_2 - \delta c_3$. In order to maintain constant composition of the binary solvent, the requirement $\delta c_3/\delta c_2 = c_3/c_2 = r$ must be fulfilled. Together, this gives the normalized eigenvectors

$$\underline{v}_1 = \begin{pmatrix} 0 \\ 1 \end{pmatrix}, \quad \underline{v}_2 = \frac{1}{\sqrt{1 + (1+r)^2}} \begin{pmatrix} 1 + r \\ -1 \end{pmatrix}. \tag{2}$$

The transformation matrix $\underline{\underline{\mathbf{V}}} = (\underline{v}_1, \underline{v}_2)$ contains the eigenvectors as column vectors. It allows us to transform the diffusion matrix $\underline{\underline{\hat{\mathbf{D}}}}$, that is, diagonal in the directions of the two eigenvectors, back to the concentration space of Eq. (1),

$$\underline{\underline{\mathbf{D}}} = \underline{\underline{\mathbf{V}}} \begin{pmatrix} \hat{D}_1 & 0 \\ 0 & \hat{D}_2 \end{pmatrix} \underline{\underline{\mathbf{V}}}^{-1} = \begin{pmatrix} \hat{D}_2 & 0 \\ \dfrac{\hat{D}_1 - \hat{D}_2}{1+r} & \hat{D}_1 \end{pmatrix}. \tag{3}$$

Since the solvent interdiffusion is much faster than the polymer diffusion, $\hat{D}_1 \gg \hat{D}_2$, the off-diagonal diffusion coefficient $D_{21}$ is of similar magnitude as the diagonal ones.

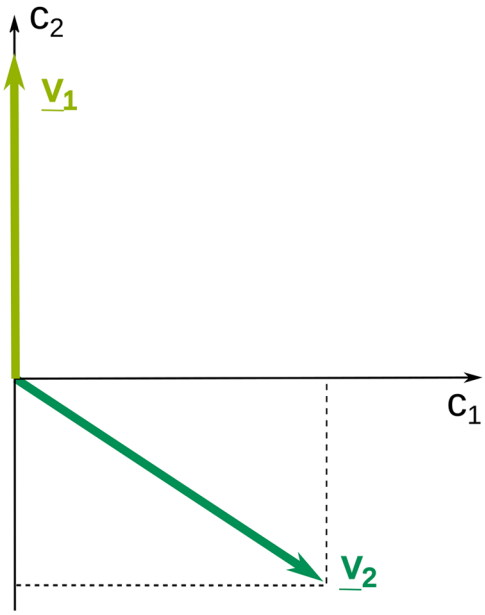


**FIG. 2.** Eigenvectors of the diffusion matrix in the $(c_1, c_2)$-space for the case $r = c_3/c_2 = 0.5$.

## B. Optical measurement

The signals recorded in a two-color optical experiment are written in Ref. 4 after normalization to the amplitude of the respective thermal contribution in the general form

$$\underline{s}^{\text{norm}}(t) = \underline{1} + \underline{\underline{\mathbf{M}}}\,\underline{f}(t), \tag{4}$$

where $\underline{s}^{\text{norm}}(t) = (s_1^{\text{norm}}(t), s_2^{\text{norm}}(t))^{\text{T}}$ is a column vector with the signals for the two detection wavelengths $\lambda_1$ and $\lambda_2$. The vector $\underline{f}(t) = (f_1(t), f_2(t))^{\text{T}}$ contains the two transients $f_j(t)$ that start at zero for $t = 0$ and approach unity for $t \to \infty$. The characteristic rise time $t_j$ of $f_j(t)$ is determined by the diffusion eigenvalue $\hat{D}_j$. The detailed mathematical form of $f_j(t)$ depends on the type of experiment performed and differs between, e.g., TDFRS and OBD.[4] Together with the $2 \times 2$ amplitude matrix $\underline{\underline{\mathbf{M}}}$, this results in a bimodal rise with amplitudes $\mathrm{M}_{i1}$ and $\mathrm{M}_{i2}$ of the signals $s_i^{\text{norm}}(t)$ recorded with wavelengths $\lambda_i$. The two-color measurements are then evaluated by fitting Eq. (4) to obtain the two diffusion eigenvalues $\hat{D}_j$ and the four entries $\mathrm{M}_{ij}$ of the amplitude matrix, which is related to the concentration changes in the eigenspace of the diffusion matrix by

$$\underline{\underline{\mathbf{M}}} = \frac{1}{\delta T}\underline{\underline{\mathbf{N_T}}}^{-1}\underline{\underline{\mathbf{N_c}}}\,\underline{\underline{\mathbf{V}}}\,\underline{\underline{\delta\mathbf{C}}}_{\infty}. \tag{5}$$

Here, $\delta T$ is the applied temperature difference, $\underline{\underline{\mathbf{N_T}}}$ is the diagonal matrix with the thermal contrast factors $N_{T,ij} = (\partial n_i/\partial T)_{c_1,c_2,p}\,\delta_{ij}$, and $\underline{\underline{\mathbf{N_c}}}$ is the matrix with the solutal contrast factors $N_{c,ij} = (\partial n_i/\partial c_j)_{c_{k\neq j},T,p}$. The refractive index $n_i$ is measured at the respective detection wavelength $\lambda_i$. The diagonal matrix $\underline{\underline{\delta\mathbf{C}}}_{\infty}$ contains the two steady state amplitudes $\delta C_{\infty,j}$ in the directions of the two eigenvectors $\underline{v}_j$ of $\underline{\underline{\mathbf{D}}}$. They are transformed into the space of the independent concentrations $c_1$ and $c_2$ by $\underline{\delta c} = \underline{\underline{\mathbf{V}}}\,\underline{\underline{\delta\mathbf{C}}}_{\infty}\underline{1}$, where $\underline{1} = (1,1)^{\text{T}}$. The four amplitudes $\mathrm{M}_{ij}$ and the two diffusion eigenvalues are the basis for any subsequent analysis. They characterize the experiment completely and are everything that can directly be extracted from a two-color measurement on a ternary mixture.

Before we proceed, it is instructive to take a brief look at the established standard data evaluation for ternary mixtures, where the diffusion eigenvectors and, hence, the transformation matrix $\underline{\underline{\mathbf{V}}}$ are not known. The computation of the concentration changes $\underline{\delta c}$ from Eq. (5) requires the inversion of the frequently ill-conditioned contrast factor matrix $\underline{\underline{\mathbf{N_c}}}$.[9] Using this standard procedure, the diffusion matrix and the primed Soret coefficients would be calculated as[4]

$$\underline{\underline{\mathbf{D}}} = (\underline{\underline{\mathbf{N_c}}}^{-1}\,\underline{\underline{\mathbf{N_T}}}\,\underline{\underline{\mathbf{M}}})\,\underline{\underline{\hat{\mathbf{D}}}}\,(\underline{\underline{\mathbf{M}}}^{-1}\underline{\underline{\mathbf{N_T}}}^{-1}\underline{\underline{\mathbf{N_c}}}), \tag{6}$$

$$\underline{S_T'} = -\underline{\underline{\mathbf{N_c}}}^{-1}\underline{\underline{\mathbf{N_T}}}\,\underline{\underline{\mathbf{M}}}\,\underline{1}. \tag{7}$$

By comparing Eqs. (3) and (6), we can identify the transformation matrix as $\underline{\underline{\mathbf{V}}} = \underline{\underline{\mathbf{N_c}}}^{-1}\underline{\underline{\mathbf{N_T}}}\,\underline{\underline{\mathbf{M}}}$. However, this is not the route we want to follow here because of the aforementioned problematic inversion of $\underline{\underline{\mathbf{N_c}}}$. We will come back to the problem of the inversion of the contrast factor matrix for the determination of the eigenvectors of $\underline{\underline{\mathbf{D}}}$ in the last part of the manuscript.

The huge advantage of our new procedure is the *a priori* knowledge of the two eigenvectors. This avoids the inversion of $\underline{\underline{\mathbf{N_c}}}$, and the two $\delta C_{\infty,j}$ $(j = 1, 2)$ are directly obtained from a single wavelength $\lambda_i$ according to Eq. (5),

$$\delta C_{\infty,j} = \frac{M_{ij}\,\delta T}{V_{1j}N_{c,i1}/N_{T,ii} + V_{2j}N_{c,i2}/N_{T,ii}}. \tag{8}$$

Because of the additional *a priori* knowledge, a measurement with one wavelength is sufficient. In the case of a two-color experiment, Eq. (8) holds for either wavelength $\lambda_1$ or $\lambda_2$, which both should yield identical $\delta C_{\infty,j}$.

Next, we can calculate the actual concentration changes associated with the fast and the slow mode. Since we have chosen $\hat{D}_1$ as the eigenvalue of the fast mode with amplitude $\delta C_{\infty,1}$, the concentration changes in terms of the independent concentrations $c_1$ and $c_2$ become

$$\underline{\delta c}^{\text{fast}} = \underline{\underline{\mathbf{V}}}\begin{pmatrix}\delta C_{\infty,1}\\ 0\end{pmatrix} = \delta C_{\infty,1}\begin{pmatrix}V_{11}\\ V_{21}\end{pmatrix}. \tag{9}$$

Correspondingly, for the slow mode,

$$\underline{\delta c}^{\text{slow}} = \underline{\underline{\mathbf{V}}}\begin{pmatrix}0\\ \delta C_{\infty,2}\end{pmatrix} = \delta C_{\infty,2}\begin{pmatrix}V_{12}\\ V_{22}\end{pmatrix}. \tag{10}$$

Figure 3 visualizes the concentration changes associated with the fast and the slow mode for a mixture with $r = c_3/c_2 = 0.5$. The fast mode with characteristic time $t_1$ describes the diffusion of $c_2$ with respect to $c_3$ at constant $c_1$, the solvent interdiffusion. The

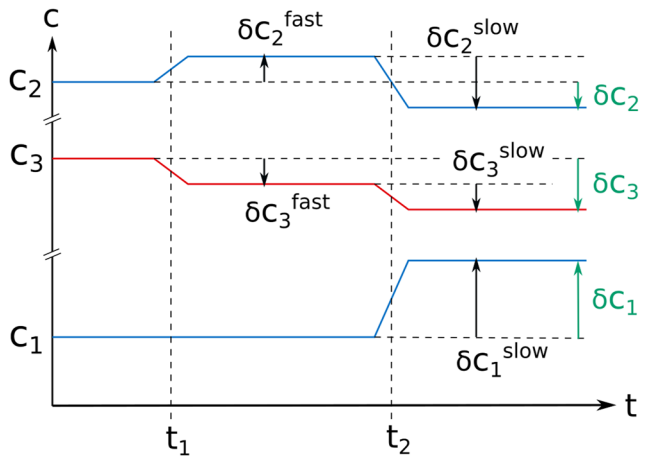


**FIG. 3.** The independent concentrations are $c_1$ and $c_2$, while $c_3$ is the dependent one. In the chosen example with $r = c_3/c_2 = 0.5$, the concentration $c_2$ even changes its sign during the slow mode.

slow mode with characteristic time $t_2$ is the diffusion of $c_1$, the polymer, with respect to the mixed solvent of constant composition. In the space of the independent concentrations $c_1$ and $c_2$, the changes in the dependent concentration $c_3$ are not explicitly considered and the eigenvectors point in the directions associated with the two modes, hence $\underline{v_1} \sim (0, \delta c_2^{\text{fast}})^{\text{T}}$ and $\underline{v_2} \sim (\delta c_1^{\text{slow}}, \delta c_2^{\text{slow}})^{\text{T}}$. Finally, $\delta c_i = \delta c_i^{\text{fast}} + \delta c_i^{\text{slow}}$ is the total concentration change of the respective component in the nonequilibrium steady state for $t \to \infty$.

### C. The Soret coefficients

The so-called primed Soret coefficients, which are frequently employed for ternary mixtures[18] and which are also considered in Eq. (7), are readily obtained from the total asymptotic concentration changes as

$$S'_{T,i} = -\frac{\delta c_i}{\delta T}, \tag{11}$$

which automatically satisfy the relation $\sum_{i=1}^{3} S'_{T,i} = 0$.

Instead of the primed Soret coefficients, the Soret coefficient $S_T$ of a binary mixture with concentration $c$ of the independent component is usually defined with concentration prefactors, i.e., $S_T = -[c(1-c)]^{-1}\delta c/\delta T = [c(1-c)]^{-1} S'_T$. This definition bears two distinct advantages. First, $S_T$ becomes finite and independent of $c$ in the two dilute limits whereas $S'_T$ increases proportional to $c$ or $(1-c)$, respectively. Second, $S_T$ is, other than $S'_T$, invariant under transformation from a mole fraction to a mass fraction based representation of the concentrations.[19]

The use of the primed coefficients for ternary systems was largely owed to a lack of knowledge about how transformation-invariant coefficients should be defined for ternaries. It was only in 2019 that Ortiz de Zárate derived concentration prefactors that yield frame-invariant Soret coefficients also in the ternary case.[19] They are related to the primed coefficients by

$$\begin{pmatrix} S_{T,1} \\ S_{T,2} \end{pmatrix} = \begin{pmatrix} c_1(1-c_1) & -c_1 c_2 \\ -c_1 c_2 & c_2(1-c_2) \end{pmatrix}^{-1} \begin{pmatrix} S'_{T,1} \\ S'_{T,2} \end{pmatrix}. \tag{12}$$

The assignment of the diffusion eigenvectors in Fig. 2 breaks the entire separation down into two successive steps along different directions in the composition space that both can be regarded as quasi-binary: the fast mode is the quasi-binary diffusion of $c_2$ with respect to $c_3$ at fixed $c_1$ and the slow mode is the quasi-binary diffusion of $c_1$ with respect to the mixed solvent of constant composition $c_2/c_3$. It is straightforward to assign primed Soret coefficients to all three components separately for the following two modes:

$$S'^{\text{fast}}_{T,i} = -\delta c_i^{\text{fast}}/\delta T, \tag{13}$$

$$S'^{\text{slow}}_{T,i} = -\delta c_i^{\text{slow}}/\delta T. \tag{14}$$

They are related to the total primed coefficients by $S'^{\text{fast}}_{T,i} + S'^{\text{slow}}_{T,i} = S'_{T,i}$.

Since the two modes correspond to quasi-binary diffusion, effective binary Soret coefficients (without the "prime") can be defined for the fast and the slow modes with the proper binary concentration prefactors as

$$S^{\text{fast}}_{T,2} = -S^{\text{fast}}_{T,3} = -\frac{\delta c_2^{\text{fast}}}{\delta T}\frac{1}{c_2 c_3}, \tag{15}$$

$$S^{\text{slow}}_{T,1} = -\frac{\delta c_1^{\text{slow}}}{\delta T}\frac{1}{c_1(c_2+c_3)}. \tag{16}$$

The concentration prefactor $c_2 c_3$ for the fast mode takes only the two diffusing solvents into account but not the inert polymer, which is immobile on time scales associated with $t_1$. The prefactor for the slow mode, $c_1(c_2+c_3) = c_1(1-c_1)$, accounts for the diffusing polymer and the mixed solvent of total weight fraction $c_2 + c_3 = 1 - c_1$.

## III. EXPERIMENTAL

The ternary samples were solutions of polystyrene (PS, Polymer Standards Service GmbH, article PSS-ps4.5k, lot ps150410, $M_w = 4880$ g/mol, $M_n = 4700$ g/mol, $M_p = 4840$ g/mol) dissolved in a mixture of toluene (Tol, VWR AnalaR NORMAPUR, article 28 676.297, lot 20E044015, purity >99.5%) and cyclohexane (cHex, VWR AnalaR NORMAPUR, article 23 224.293, lot 18F074018, purity >99.5%). The numbering of the components is PS/Tol/cHex as $c_1/c_2/c_3$ with $c_3$ (cHex) as the dependent component. The sample composition in mass fractions PS/Tol/cHex was 0.040/0.480/0.480, hence $r = c_3/c_2 = 1$.

Measurements were performed by means of two-color optical beam deflection (2-OBD)[4,6,7] with a Soret cell of $h = 1.20$ mm height. The employed vacuum laser wavelengths are $\lambda_1 = 405.0$ nm and $\lambda_2 = 632.8$ nm. The measurements were carried out under ambient pressure at four different temperatures between $T = 293.15$ K and 308.15 K ($\theta = 20$–$35\,^\circ$C).

The optical contrast factors are listed in Table I. They are required to calculate the concentration changes along the directions

**TABLE I.** Solutal $\partial_{c_j} n(\lambda_i) = \left(\partial n(\lambda_i)/\partial c_j\right)_{p,T,c_{k\neq j}}$ and thermal $\partial_T n(\lambda_i) = \left(\partial n(\lambda_i)/\partial T\right)_{p,c_1,c_2}$ contrast factors. The first row contains the condition number of the solutal contrast factor matrix. The two independent concentrations are PS ($c_1$) and Tol ($c_2$). Statistical error of solutal contrast factors: $\sigma \approx 0.0003$. Total error of solutal contrast factors: $\sigma \approx 0.001$. Error of thermal contrast factors: $\sigma \approx 1.0 \times 10^{-6}$ K$^{-1}$. System PS/Tol/cHex with composition 0.040/0.480/0.480.

| $\lambda$/nm | | Units | 20 °C | 25 °C | 30 °C | 35 °C |
|---|---|---|---|---|---|---|
| | cond($\underline{\mathbf{N}_c}$) | 1 | 55 | 55 | 56 | 56 |
| 405.0 | $\partial_{c_1} n(\lambda_1)$ | 1 | 0.1743 | 0.1749 | 0.1755 | 0.1761 |
| 405.0 | $\partial_{c_2} n(\lambda_1)$ | 1 | 0.0883 | 0.0881 | 0.0880 | 0.0878 |
| 632.8 | $\partial_{c_1} n(\lambda_2)$ | 1 | 0.1527 | 0.1534 | 0.1540 | 0.1547 |
| 632.8 | $\partial_{c_2} n(\lambda_2)$ | 1 | 0.0705 | 0.0704 | 0.0703 | 0.0703 |
| 405.0 | $\partial_T n(\lambda_1)$ | $10^{-4}$ K$^{-1}$ | −5.75 | −5.77 | −5.78 | −5.80 |
| 632.8 | $\partial_T n(\lambda_2)$ | $10^{-4}$ K$^{-1}$ | −5.48 | −5.49 | −5.51 | −5.53 |

of the diffusion eigenvectors according to Eq. (8). The solutal ones were measured as usual[20] from a concentration series in the ternary composition space and a polynomial fit of the refractive index as a function of the two independent concentrations $c_1$ and $c_2$ for both employed wavelengths. The thermal contrast factors were measured interferometrically as described in Refs. 21 and 22.

## IV. RESULTS

Figure 4 shows the solutal part of an OBD signal for the blue (405.0 nm) laser. The simultaneous measurement for the red (63 2.8 nm) laser looks similar and is not explicitly shown. The data evaluation was performed as described in Ref. 23, and the Taylor

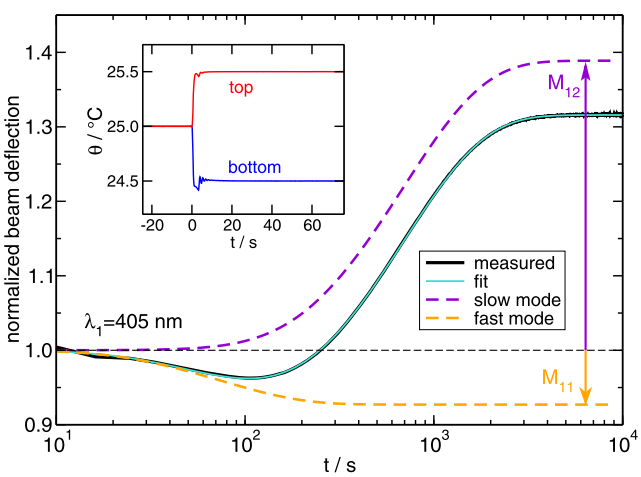


**FIG. 4.** Solutal part of the OBD beam deflection signal for the blue laser ($\lambda_1$ = 405.0 nm) after normalization to the fast thermal contribution. The dashed curves are the fast and the slow modes plotted separately. The insert shows the recorded temperatures of the top and the bottom plates, which reach their steady state values ~10–20 s after the switching. System PS/Tol/cHex with composition 0.040/0.480/0.480. Temperature $\theta$ = 25 °C.

**TABLE II.** Amplitude matrix elements $M_{ij}$ and diffusion eigenvalues $\hat{D}_j$ for the OBD-measurements with $\lambda_1$ = 405.0 nm and $\lambda_2$ = 632.8 nm. Error of amplitude matrix elements: $\sigma \approx 0.002$. Error of diffusion eigenvalues: $\sigma \approx 0.2 \times 10^{-10}$ m$^2$/s. System PS/Tol/cHex with composition 0.040/0.480/0.480.

| | Units | 20 °C | 25 °C | 30 °C | 35 °C |
|---|---|---|---|---|---|
| $M_{11}$ | 1 | −0.078 | −0.073 | −0.070 | −0.067 |
| $M_{12}$ | 1 | 0.408 | 0.389 | 0.371 | 0.351 |
| $M_{21}$ | 1 | −0.080 | −0.076 | −0.073 | −0.071 |
| $M_{22}$ | 1 | 0.396 | 0.377 | 0.360 | 0.341 |
| $\hat{D}_1$ | $10^{-10}$ m$^2$/s | 17.2 | 19.7 | 21.1 | 24.8 |
| $\hat{D}_2$ | $10^{-10}$ m$^2$/s | 1.9 | 2.1 | 2.3 | 2.5 |

algorithm[24] was used for all data fitting. In a first step, the time-dependent OBD signals were fitted with Eq. (4) to obtain the two eigenvalues $\hat{D}_j$ of the diffusion matrix and the four entries $M_{ij}$ of the amplitude matrix in Eq. (5). The values are listed in Table II. The larger eigenvalue $\hat{D}_1$ corresponds to the fast mode, i.e., the interdiffusion of Tol and cHex, whereas $\hat{D}_2$ describes the slower diffusion of the polymer PS relative to the mixed solvent. Both contributions are plotted separately in Fig. 4 for illustration. The two amplitudes $M_{11} < 0$ and $M_{12} > 0$ of the fast and the slow mode are indicated.

The four entries of the diffusion matrix [Eq. (3)] are given in Table III. While $D_{12}$ vanishes, the off-diagonal element $D_{21}$ is of the same order of magnitude as the two diffusion eigenvalues. The postulate that the slow mode corresponds to the diffusion of component 1 with respect to the mixed solvent at constant composition $c_3/c_2 = r$ = const, and not at $c_2$ = const, is responsible for the cross-coupling of the two independent components during the slow mode and leads to the large off-diagonal matrix element $D_{21}$ in Eq. (3). Thus, this finite cross-diffusion coefficient is not negligible and at the same time not an indication of a particular interaction between the two independent components as sometimes claimed in the literature.[25] It is rather a necessary consequence of the *absence* of such interactions since the polymer diffusion does not interfere with the solvent composition in one or the other way.

The two diagonalized concentration changes $\delta C_{\infty,j}$ from Eq. (8) can be calculated for either wavelength $\lambda_i$. We have found that the values from the two wavelengths deviate by $(0.5 \ldots 1.0) \times 10^{-4}$, which translates to ~5 percent for the slow mode ($j = 2$) and less than 20 percent for the fast mode ($j = 1$). Since, after fixing the directions of the diffusion eigenvectors, the calculation

**TABLE III.** Entries of the diffusion matrix [Eq. (3)]. Error of diffusion coefficients: $\sigma \approx 0.2 \times 10^{-10}$ m$^2$/s. System PS/Tol/cHex with composition 0.040/0.480/0.480.

| | Units | 20 °C | 25 °C | 30 °C | 35 °C |
|---|---|---|---|---|---|
| $D_{11}$ | $10^{-10}$ m$^2$/s | 1.9 | 2.1 | 2.3 | 2.5 |
| $D_{12}$ | $10^{-10}$ m$^2$/s | 0.0 | 0.0 | 0.0 | 0.0 |
| $D_{21}$ | $10^{-10}$ m$^2$/s | 7.6 | 8.8 | 9.4 | 11.1 |
| $D_{22}$ | $10^{-10}$ m$^2$/s | 17.2 | 19.7 | 21.1 | 24.8 |

**TABLE IV.** Primed ternary Soret coefficients for the fast and slow modes individually. System PS/Tol/cHex with composition 0.040/0.480/0.480. Error $\sigma \approx 0.1 \times 10^{-3}$ K$^{-1}$ for the fast mode and $\sigma \approx 0.05 \times 10^{-3}$ K$^{-1}$ for the slow mode.

| | Units | 20 °C | 25 °C | 30 °C | 35 °C |
|---|---|---|---|---|---|
| $S'^{\text{fast}}_{T,1}$ | $10^{-3}$ K$^{-1}$ | 0. | 0. | 0. | 0. |
| $S'^{\text{fast}}_{T,2}$ | $10^{-3}$ K$^{-1}$ | −0.57 | −0.54 | −0.52 | −0.50 |
| $S'^{\text{fast}}_{T,3}$ | $10^{-3}$ K$^{-1}$ | 0.57 | 0.54 | 0.52 | 0.50 |
| $S'^{\text{slow}}_{T,1}$ | $10^{-5}$ K$^{-1}$ | 1.82 | 1.73 | 1.65 | 1.56 |
| $S'^{\text{slow}}_{T,2}$ | $10^{-5}$ K$^{-1}$ | −0.91 | −0.87 | −0.83 | −0.78 |
| $S'^{\text{slow}}_{T,3}$ | $10^{-5}$ K$^{-1}$ | −0.91 | −0.87 | −0.83 | −0.78 |

**TABLE V.** Primed ternary Soret coefficients for the asymptotic total separation. Top: pseudo-binary evaluation. Bottom: standard ternary evaluation according to Eq. (7). System PS/Tol/cHex with composition 0.040/0.480/0.480. Error $\sigma \approx 0.1 \times 10^{-3}$ K$^{-1}$ (pseudo-binary) and $\sigma \approx 1.0 \times 10^{-3}$ K$^{-1}$ (standard ternary).

| | | Units | 20 °C | 25 °C | 30 °C | 35 °C |
|---|---|---|---|---|---|---|
| Pseudo-binary | $S'_{T,1}$ | $10^{-3}$ K$^{-1}$ | 1.82 | 1.73 | 1.65 | 1.56 |
| | $S'_{T,2}$ | $10^{-3}$ K$^{-1}$ | −1.48 | −1.40 | −1.34 | −1.28 |
| | $S'_{T,3}$ | $10^{-3}$ K$^{-1}$ | −0.34 | −0.33 | −0.31 | −0.28 |
| Standard ternary | $S'_{T,1}$ | $10^{-3}$ K$^{-1}$ | 1.55 | 1.45 | 1.38 | 1.25 |
| | $S'_{T,2}$ | $10^{-3}$ K$^{-1}$ | −0.92 | −0.81 | −0.77 | −0.62 |
| | $S'_{T,3}$ | $10^{-3}$ K$^{-1}$ | −0.63 | −0.64 | −0.61 | −0.62 |

from both wavelengths is redundant, we have averaged the results. The discrepancy between both values is the major source of the errors for the various Soret coefficients reported in the following tables.

With the diagonalized concentration changes from Eq. (8), the concentration changes of the two independent compositions during the fast and the slow mode are obtained according to Eqs. (9) and (10). Finally, Eqs. (13) and (14) yield the ternary primed Soret coefficients for the two individual modes. Their values are listed in Table IV.

Table V lists in the upper three rows all total primed Soret coefficients for the here discussed pseudo-binary data evaluation based on the fixed diffusion eigenvectors [Eq. (11)]. The lower three rows contain the same coefficients as obtained from a standard ternary data evaluation based on the contrast factor matrix inversion without further assumptions [Eq. (7)].

The transformation-invariant ternary Soret coefficients for the total steady state separation [(Eq. (12) together with $S'_{T,i}$ from Table V, pseudo-binary] and the quasi-binary Soret coefficients for the two individual modes [Eqs. (15) and (16)] are listed in Table VI.

**TABLE VI.** Transformation-invariant ternary (top) and quasi-binary (bottom) Soret coefficients. See the text for details. System PS/Tol/cHex with composition 0.040/0.480/0.480. Errors estimated from errors of the primed Soret coefficients.

| | Units | 20 °C | 25 °C | 30 °C | 35 °C | $\sigma$ |
|---|---|---|---|---|---|---|
| $S_{T,1}$ | $10^{-3}$ K$^{-1}$ | 46.3 | 44.0 | 41.9 | 39.6 | 2.5 |
| $S_{T,2}$ | $10^{-3}$ K$^{-1}$ | −2.36 | −2.24 | −2.15 | −2.09 | 0.15 |
| $S^{\text{fast}}_{T,2}$ | $10^{-3}$ K$^{-1}$ | −2.46 | −2.33 | −2.24 | −2.17 | 0.4 |
| $S^{\text{fast}}_{T,3}$ | $10^{-3}$ K$^{-1}$ | 2.46 | 2.33 | 2.24 | 2.17 | 0.4 |
| $S^{\text{slow}}_{T,1}$ | $10^{-3}$ K$^{-1}$ | 47.5 | 45.2 | 43.0 | 40.6 | 2.5 |

## V. DISCUSSION

### A. Accuracy and stability of results

As can be seen from Table V, the primed Soret coefficients obtained by the ternary and the new pseudo-binary evaluation procedure are of comparable magnitude, but they also show notable deviations. In order to better understand the influence of experimental errors, we have performed Monte Carlo simulations with Gaussian random noise on all relevant measured parameters. The noise terms have zero mean and a standard deviation $\sigma$ that corresponds to best estimates of the experimental uncertainties of the respective quantities. In detail, we have chosen $\sigma = 0.002$ for the amplitude matrix elements $M_{ij}$ in Table II, $\sigma = 0.001$ for the solutal contrast factors $\partial_{c_j} n(\lambda_i)$, and $\sigma = 1.0 \times 10^{-6}$ K$^{-1}$ for the thermal contrast factors $\partial_T n(\lambda_i)$ in Table I. The standard deviations correspond to a confidence level of ~68% for normally distributed values. These numbers are certainly worth being discussed. In particular, both for the amplitudes and the solutal contrast factors, it is very difficult to discriminate between uncorrelated and correlated errors of the four matrix elements. Knowing about this problem, we have focused on the effect of random errors.

Figure 5 shows the primed Soret coefficients of the two independent concentrations obtained by the two evaluation methods at $\theta = 25$ °C. The large symbols are the measured Soret coefficients from Table V. The small symbols correspond to 2000 simulated values with the random errors of the experimental data.

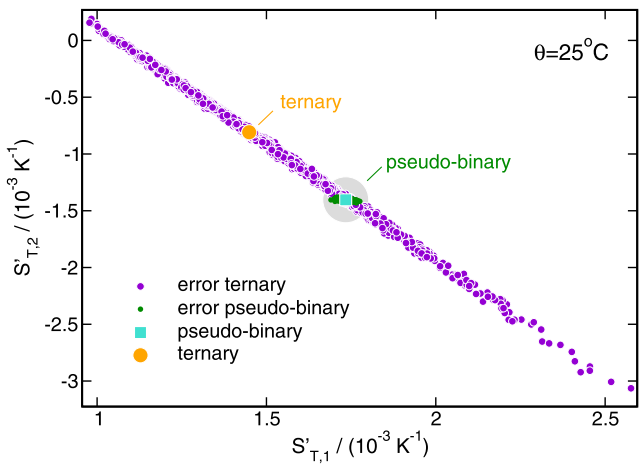


**FIG. 5.** Monte Carlo simulations of the effect of Gaussian statistical noise for the measured input parameters $M_{ij}$, $\partial_{c_j} n(\lambda_i)$, and $\partial_T n(\lambda_i)$ on the primed Soret coefficients. The effect is large for the standard ternary and small for the pseudo-binary evaluation method. See the text for details. System PS/Tol/cHex with composition 0.040/0.480/0.480. Temperature $\theta = 25$ °C.

The effect on the standard ternary evaluation is drastic. The Soret coefficients that are all compatible with the measurement within our assumed error bars spread out over an elongated ellipsoid-like region in the $S'_{T,1}$-$S'_{T,2}$-plane. The minor and the major axes of the ellipse are determined by the right-singular vectors of the contrast factor matrix $\underline{\underline{\mathbf{N_c}}}$.[9] A perfect ellipse is only to be expected in the linear approximation. For larger errors, as in our case, it becomes asymmetric and is no longer centered around the original (ternary) data point.

There are two important observations. First, the data point for the pseudo-binary model falls perfectly onto the ellipse and both results are compatible within the experimental error bars. Second, the fluctuations of the input data have only very little effect on the pseudo-binary model, where all simulation data end up within the small circle with the gray background around the original data point. Thus, stability of the pseudo-binary model against the input errors is of linear order and not larger than for measurements on binary mixtures. In summary, this allows the conclusion that the pseudo-binary results are much better approximations to the true values than the ones from the standard ternary evaluation, provided that the pseudo-binary model is indeed applicable.

From the Monte Carlo simulation, we estimate the errors of the primed Soret coefficients to $\sigma \approx 0.05 \times 10^{-3}$ K$^{-1}$ for the pseudo-binary evaluation and to $\sigma \approx 0.5 \times 10^{-3}$ K$^{-1}$ for the standard ternary evaluation. It needs to be kept in mind, however, that the errors of the three Soret coefficients are highly correlated in the latter case.

## B. Comparison with binary mixtures

In order to compare the results for the ternary polymer solution with data for binary mixtures, a number of additional data for the latter are required. They have been aggregated in Table VII and will be addressed in the following discussion.

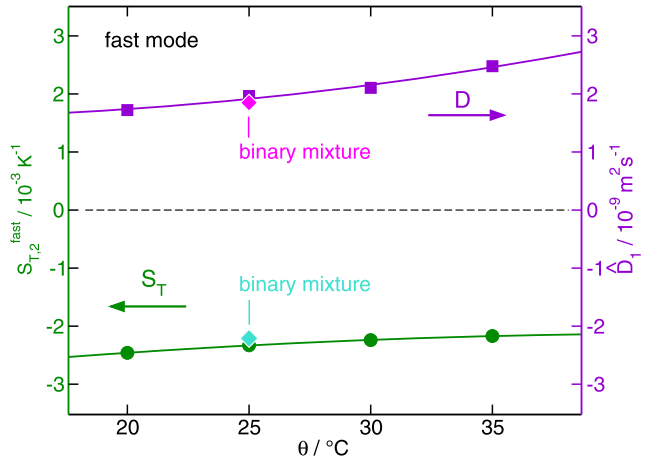


**FIG. 6.** Coefficients for the fast mode of the ternary system PS/Tol/cHex with composition 0.040/0.480/0.480 in comparison with the ones of the binary mixture Tol/cHex with composition 0.500/0.500 at $\theta$ = 25 °C. Diffusion eigenvalues $\hat{D}_1$ of the fast mode and $D$ of the binary mixture (top). Soret coefficient $S_{T,2}^{\text{fast}}$ and $S_T$ of the binary mixture (bottom).

### 1. The fast mode

First, we want to discuss the fast mode, which we attribute to the interdiffusion of the two solvents. The temperature dependence of the two corresponding transport coefficients, the diffusion eigenvalue $\hat{D}_1$ (Table II), and the Soret coefficient $S_{T,2}^{\text{fast}}$ (Table VI) are plotted in Fig. 6 for the four measured temperatures. Both quantities can nicely be fitted with only little scatter by second order polynomials.

**TABLE VII.** Transport properties for related binary mixtures. Soret and diffusion coefficients have been measured by single-color OBD in our own laboratory. The viscosity data have been extracted from Ref. 26. They are all to be understood as the viscosities of the solvents or solvent mixtures, not of the entire polymer solutions. The viscosity $\eta_{sol}$ is the one of the symmetric binary solvent mixture Tol/cHex. Temperature $\theta$ = 25 °C.

| System | Quantity | Units | Value | $\sigma$ |
|---|---|---|---|---|
| Tol/cHex | $S_T$ | $10^{-3}$ K$^{-1}$ | −2.21 | 0.05 |
| 0.500/0.500 | $D$ | $10^{-10}$ m$^2$s$^{-1}$ | 18.5 | 0.5 |
| PS/Tol | $S_T$ | $10^{-3}$ K$^{-1}$ | 43.0 | 1.0 |
| 0.040/0.960 | $D$ | $10^{-10}$ m$^2$s$^{-1}$ | 2.48 | 0.1 |
| | $\eta_{Tol}$ | mPa·s | 0.566 | 0.005 |
| | $\eta_{Tol}D$ | $10^{-10}$ (m$^2$ s$^{-1}$) (mPa s) | 1.41 | 0.06 |
| PS/cHex | $S_T$ | $10^{-3}$ K$^{-1}$ | 47.9 | 1.0 |
| 0.040/0.960 | $D$ | $10^{-10}$ m$^2$ s$^{-1}$ | 1.25 | 0.1 |
| | $\eta_{cHex}$ | mPa s | 0.906 | 0.008 |
| | $\eta_{cHex}D$ | $10^{-10}$ (m$^2$ s$^{-1}$) (mPa s) | 1.136 | 0.09 |
| PS/Tol/cHex | $\eta_{sol}$ | mPa s | 0.599 | 0.01 |
| 0.040/0.480/0.480 | $\eta_{sol}\hat{D}_2$ | $10^{-10}$ (m$^2$ s$^{-1}$) (mPa s) | 1.27 | 0.12 |

As a test of our assumption, we have also measured the symmetric binary mixture Tol/cHex with 0.500/0.500 mass fractions at $\theta = 25\,^{\circ}\mathrm{C}$. For the binary mixture, the conventional single-color OBD technique could be employed. Contrary to the more complicated two-color experiments on ternary mixtures, the measurements for binaries are straightforward, and a detailed description has been given elsewhere.[22] Both determined coefficients of the binary mixture, which are listed in the first two rows of Table VII, are included in Fig. 6. The agreement with the corresponding coefficients for the fast mode is convincing.

### 2. The slow mode

Next, we come to the slow mode, which we attribute to the polymer diffusion. Figure 7 shows, in a similar plot as before, the diffusion eigenvalue $\hat{D}_2$ of the slow mode and the effective binary Soret coefficient $S_{T,1}^{\mathrm{slow}}$ of the polymer (Table VI) for the measured temperatures. In addition, the data fall almost perfectly onto second order polynomial fits with very little scatter.

Similar to the slow mode, we have performed additional measurements for related binary mixtures, which are in this case the solutions of the polymer in the pure solvents at the same polymer concentration $c_1 = 0.04$. The numerical values of the Soret and diffusion coefficients are listed in Table VII. Other than for the fast mode, the data from the binary solutions are not expected to coincide with their ternary counterparts, but they nicely frame the latter. The Soret coefficient $S_{T,1}^{\mathrm{slow}}$ of the ternary system almost perfectly interpolates between the Soret coefficients $S_T$ of the two binary limits.

Finally, we observe in Table VI that the transformation-invariant Soret coefficient of Tol, $S_{T,2}$, is in excellent agreement with the Soret coefficient of the binary mixture Tol/cHex and the one of the fast mode in Fig. 6. Furthermore, the transformation-invariant Soret coefficient of PS, $S_{T,1}$, agrees well with the Soret coefficient $S_{T,1}^{\mathrm{slow}}$ of the slow mode and the value interpolated from the two polymer solutions in the pure solvents (Fig. 7).

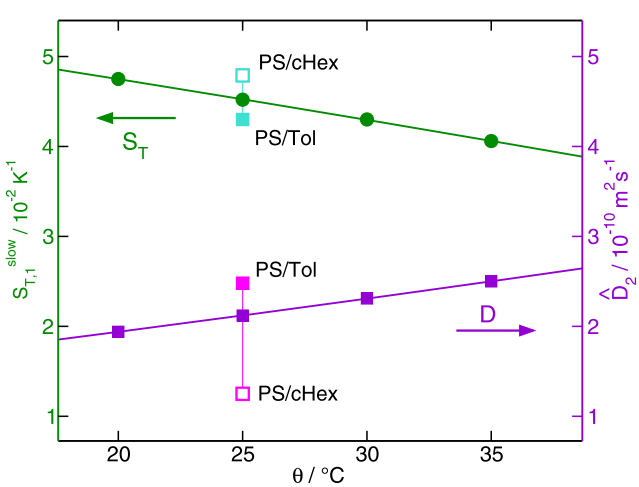


**FIG. 7.** Coefficients for the slow mode of the ternary system PS/Tol/cHex with composition 0.040/0.480/0.480 in comparison with the ones of the binary polymer solutions PS/Tol and PS/cHex with compositions of 0.040/0.960. Soret coefficient $S_{T,1}^{\mathrm{slow}}$ and $S_T$ of the binary mixture (top). Diffusion eigenvalues $\hat{D}_2$ of the slow mode and $D$ of the binary mixture (bottom).

The situation is different and more complicated for the diffusion coefficient, where $\hat{D}_2$ is much closer to the value for PS/Tol and not approximately given by the mean values of the two binary diffusion coefficients.

A major impact on polymer diffusion coefficients in dilute to semidilute solutions stems from the solvent viscosity. Its influence can be scaled out by looking at the products $\eta D$ instead of $D$ alone. The viscosities of the pure solvents and of the Tol/cHex-mixture can be extracted from Ref. 26, where a mixing rule for the viscosity, based on mole fractions $x_i$, is given as

$$\eta_{mix} = \sum_{i=1}^{2} x_i \eta_i + \Delta\eta \tag{17}$$

with a Redlich–Kister polynomial for the viscosity deviation

$$\Delta\eta = x_i x_j\left[(A_0 + A_1/T) + (B_0 + B_1/T)(x_i - x_j)\right]. \tag{18}$$

The fit coefficients for $\Delta\eta$ in mPa·s are $A_0 = 3.855$, $A_1 = -1.318 \times 10^3$ K, and $B_0 = 2.464B_1 = -0.807 \times 10^3$ K.

The viscosities of the pure and the mixed solvents, the viscosity-scaled diffusion coefficients for the two binary polymer solutions, and the viscosity-scaled slow diffusion eigenvalue $\hat{D}_2$ of the ternary system are also included in Table VII. The data are not explicitly plotted, but from the numbers it is apparent that the viscosity-scaled diffusion coefficients are much more similar and that the viscosity-scaled eigenvalue $\eta_{sol}\hat{D}_2 = \eta_{Tol/cHex}\hat{D}_2$ coincides almost perfectly with the mean value from the two binaries. Thus, the strong asymmetry of the diffusion coefficients in Fig. 7 is entirely caused by the viscosities.

### 3. The diffusion eigenvectors and the diffusion path

Finally, we want to shed some additional light on the diffusion eigenvectors. As we have seen in Fig. 5, the Soret coefficients obtained by the full ternary and by the pseudo-binary evaluation method agree fairly well, albeit the ternary method suffers from large anisotropic errors caused by the ill-conditioned contrast factor matrix. Since the *a priori* assumption about the direction of the diffusion eigenvectors shown in Fig. 2 is at the core of our data treatment, it is instructive to take a look at the diffusion eigenvectors that result from the ternary evaluation. By slightly rewriting Eq. (5), we obtain

$$\underline{\underline{\delta\mathbf{c}}} = \delta T\, \underline{\underline{\mathbf{N_c}}}^{-1} \underline{\underline{\mathbf{N_T}}}\ \underline{\underline{\mathbf{M}}}, \tag{19}$$

where $\underline{\underline{\delta\mathbf{c}}}$ is a $2 \times 2$ matrix, whose column vectors are the concentration changes of the two independent components for the fast mode (column 1) and the slow mode (column 2). They are not normalized, but they point in the directions of the diffusion eigenvectors.

Figure 8 shows the thus obtained concentration changes for the two modes (filled violet circles) and the total concentration change (open violet circle). The green squares show the corresponding concentration changes from the pseudo-binary evaluation. They are directly calculated from the primed Soret coefficients in Table IV as $\delta c = -\delta T\, S_T'$ and, naturally, point in the directions of the chosen diffusion eigenvectors (a negative sign is of no concern).

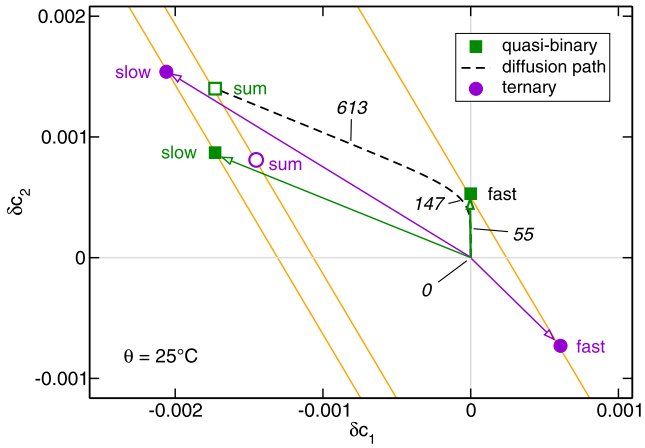


**FIG. 8.** Concentration changes during the fast and the slow mode and total concentration change (sum) as determined by the standard ternary and the quasi-binary evaluation methods. The arrows point in the directions of the diffusion eigenvectors. The orange lines indicate the direction of the long axis of the error ellipsoid in Fig. 5. The dashed line is the diffusion path, along which the position of the sample in the concentration space evolves during the transient build-up phase of the concentration gradient. The slanted numbers give the position on the diffusion path in seconds after switching on the temperature gradient. System PS/Tol/cHex with composition 0.040/0.480/0.480. Temperature $\theta = 25\,^{\circ}\mathrm{C}$.

Other than the Soret coefficients in Fig. 5, the diffusion eigenvectors are more sensitive to experimental errors and hardly show similarities at all. Nevertheless, the eigenvectors from the two evaluation methods can be considered consistent. Both for the fast and the slow mode and for the sum of both, the matching pairs of data points fall onto straight lines with the slope defined by the long axis of the error ellipsoid in Fig. 5. This example shows that the poor condition number of the contrast factor matrix, while it may still yield acceptable estimates of the Soret coefficients and the diffusion eigenvalues, can lead to completely unreliable eigenvectors of the diffusion matrix.

Thompson and Morral discussed in detail diffusion paths in isothermal ternary alloys after a perturbation and their relation to diffusion eigenvectors.[27] In our situation, with a nonequilibrium steady state, the (thermo)diffusion path in the concentration space reflects the evolution of the concentration gradients of the two independent components across the sample in the $c_1$-$c_2$-space, parameterized as a function of time.

We have plotted the diffusion path for the quasi-binary evaluation in Fig. 8 as a dashed black line. It is particularly simple due to the well separated time scales of the two modes. It first proceeds along fast eigenvector $\underline{v}_1$ towards the composition difference labeled with "fast" and then along the direction of the slow eigenvector $\underline{v}_2$ to finally reach the steady state denoted as "sum" in Fig. 8. It can be calculated as follows.

From the concentration matrix $\underline{\underline{\delta \mathbf{c}}}$ in Eq. (19) and the transients $\underline{f(t)}$ in Eq. (4), the time evolution of the two independent concentrations is given by $\underline{\delta c(t)} = (\delta c_1(t), \delta c_2(t))^{\mathrm{T}} = \underline{\underline{\delta \mathbf{c}}}\ \underline{f(t)}$. The vector $\underline{\delta c(t)}$ defines a parametric representation of the diffusion path in the concentration space. Due to the way it is calculated, $\delta c_i(t)$ is to be understood as the product of the concentration gradient in the center of the cell times the cell height. In the asymptotic limit, this quantity is identical to the concentration difference between the hot and the cold plate. For finite times, both quantities are related but not identical. The slanted numbers in Fig. 8 give the time in seconds when the respective position on the diffusion path is reached.

## VI. SUMMARY AND CONCLUSION

We have investigated thermodiffusion of a ternary system consisting of a polymer at moderate concentration in a mixed solvent by means of two-color optical beam deflection. The transformation from the experimentally accessible refractive index space to the concentration space is, as for many ternary mixtures, hampered by an ill-conditioned contrast factor matrix, which leads to a strong error amplification. Since the time dependent beam deflection signals show two well separated diffusion eigenvalues, a plausible assumption is that the fast mode can be attributed to the solvent interdiffusion and the slow mode to the polymer diffusion. Since this fixes the directions of the eigenvectors of the diffusion matrix, the stability of the data evaluation is greatly improved and on par with the situation in binary mixtures.

In the first part of our work, we have developed a so-called pseudo-binary formalism that is based on the established treatment of ternary systems, however, with a pre-defined transformation matrix between the independent concentrations $c_i$ and the concentrations $C_j$ in the diffusion eigenspace. This formalism directly leads to non-vanishing off-diagonal elements (cross-diffusion coefficients) in the diffusion matrix and allows not only the determination of the total Soret coefficients of the asymptotic steady state but also the Soret coefficients associated with the fast and the slow mode separately.

The assignment of the two modes is strongly supported by a comparison with binary mixtures. The Soret and diffusion coefficients of the fast mode agree almost perfectly with the respective coefficients for a binary mixture of the two solvents of identical composition. For the slow mode, there is no directly comparable binary system, but the Soret coefficient of the slow mode perfectly interpolates the Soret coefficients of the corresponding polymer solutions in the pure solvents. For the diffusion coefficient, the interpolation seems to be not as perfect, but this asymmetry is resolved by factoring out the viscosity effect.

While the good agreement with the results from the binary systems is a strong hint that the assignment of the diffusion eigenvectors is correct, it is, of course, not an ultimate proof. Although it looks very plausible, the interpolation of the slow mode between the polymer solutions in the pure solvents is not a strict requirement. As observed for the diffusion coefficient, the interpolation to the mixed solvent can also be non-linear. In the case of $D$, there is a trivial reason caused by the nonlinear interpolation of the viscosity.

An additional aspect we have not yet explicitly considered is the different solvent quality of toluene and cyclohexane for polystyrene. While toluene is a good solvent with a large positive second virial coefficient,[28] cyclohexane is a theta solvent with an even slightly negative second virial coefficient at $\theta = 25\,^{\circ}\mathrm{C}$ and for the employed molar mass.[29] While the effect of solvent quality

on polymer diffusion has already been studied in the literature,[30] the situation is more complicated in the case of the Soret coefficient. So far, no theory exists that would allow to relate the Soret and the thermodiffusion coefficients to the solvent quality. We are planning to specifically address the solvent quality aspect in future works.

We expect that the method can also be applied to other binary systems with different sizes of the constituents, e.g., colloidal dispersions in mixed solvents. A question that has not yet been addressed is the influence of the concentration. For the here investigated low molar mass polystyrene, the concentration can still be regarded as dilute, but for higher molar masses, the sample would be in the semidilute regime with chain overlap and entanglements. Currently, we are working on the extension of both the molar mass and the concentration range.

## ACKNOWLEDGMENTS

This work was supported by the Deutsche Forschungsgemeinschaft (Grant No. DFG, KO1541/13-1) and the Deutsches Zentrum für Luft- und Raumfahrt (DLR) (Grant No. 50WM2147). A particular thanks goes to A. Mialdun for inspiring discussions.

## AUTHOR DECLARATIONS

### Conflict of Interest

The authors have no conflicts to disclose.

### Author Contributions

**D. Sommermann**: Conceptualization (equal); Data curation (lead); Formal analysis (equal); Investigation (lead); Methodology (equal); Writing – original draft (supporting). **M. Schraml**: Conceptualization (equal); Formal analysis (supporting); Methodology (equal); Writing – review & editing (equal). **W. Köhler**: Conceptualization (equal); Formal analysis (equal); Funding acquisition (lead); Methodology (equal); Writing – original draft (lead).

## DATA AVAILABILITY

The data that support the findings of this study are available from the corresponding author upon reasonable request.

## REFERENCES

[1] S. Srinivasan and M. Z. Saghir, Int. J. Thermal Sci. **50**, 1125 (2011).
[2] W. Köhler and K. I. Morozov, J. Non-Equilib. Thermodyn. **41**, 151 (2016).
[3] M. Piszko, C. Giraudet, and A. P. Fröba, Int. J. Thermophys. **41**, 102 (2020).
[4] M. Gebhardt and W. Köhler, J. Chem. Phys. **142**, 084506 (2015).
[5] V. Shevtsova, V. Sechenyh, A. Nepomnyashchy, and J. C. Legros, Philos. Mag. **91**, 3498 (2011).
[6] K. B. Haugen and A. Firoozabadi, J. Phys. Chem. B **110**, 17678 (2006).
[7] A. Königer, H. Wunderlich, and W. Köhler, J. Chem. Phys. **132**, 174506 (2010).
[8] V. Shevtsova *et al.*, Microgravity Sci. Technol. **25**, 275 (2014).
[9] T. Triller *et al.*, Eur. Phys. J. E **42**, 27 (2019).
[10] A. Mialdun *et al.*, Eur. Phys. J. E **38**, 27 (2015).
[11] A. Mialdun, M. Bou-Ali, and V. Shevtsova, Phys. Rep. **11**, 17735 (2021).
[12] B.-J. de Gans, R. Kita, S. Wiegand, and J. Luettmer-Strathmann, Phys. Rev. Lett. **91**, 245501 (2003).
[13] L. Garcia-Fernandez *et al.*, Eur. Phys. J. E **42**, 124 (2019).
[14] W. Köhler and P. Rossmanith, J. Phys. Chem. **99**, 5838 (1995).
[15] S. Wiegand, H. Ning, and H. Kriegs, J. Phys. Chem. B **111**, 14169 (2007).
[16] A. Mialdun and V. M. Shevtsova, Int. J. Heat Mass Transfer **51**, 3164 (2008).
[17] K. B. Haugen and A. Firoozabadi, J. Chem. Phys. **124**, 054502 (2006).
[18] M. M. Bou-Ali *et al.*, Eur. Phys. J. E **38**, 30 (2015).
[19] J. M. Ortiz de Zárate, Eur. Phys. J. E **42**, 43 (2019).
[20] M. Gebhardt and W. Köhler, Eur. Phys. J. E **38**, 24 (2015).
[21] G. Wittko and W. Köhler, Philos. Mag. **83**, 1973 (2003).
[22] A. Königer, B. Meier, and W. Köhler, Philos. Mag. **89**, 907 (2009).
[23] M. Gebhardt and W. Köhler, J. Chem. Phys. **143**, 164511 (2015).
[24] H. Späth, *Algorithmen für multivariable Ausgleichsmodelle* (Oldenburg, München, 1973).
[25] R. Kita, S. Wiegand, and J. Luettmer-Strathmann, J. Chem. Phys. **121**, 3874 (2004).
[26] A. A. Silva, R. A. Reis, and M. L. L. Paredes, J. Chem. Eng. Data **54**, 2067 (2009).
[27] M. S. Thompson and J. E. Morral, Acta Metall. **34**, 339 (1986).
[28] H. Okada, S. Matsumoto, and Y. Nakamura, Polym. J. **42**, 386 (2010).
[29] H. Yamakawa, F. Abe, and Y. Einaga, Macromolecules **27**, 5704 (1994).
[30] E. Gulari, E. Gulari, Y. Tsunashima, and B. Chu, Polymer **20**, 347 (1979).